DAMTP-2016-57

A dynamical α-cluster model of ^{16}O

C. J. Halcrow*, C. King†, and N. S. Manton‡
Department of Applied Mathematics and Theoretical Physics,
University of Cambridge, Wilberforce Road, Cambridge CB3 0WA, United Kingdom
(Dated: January 17, 2017)

We calculate the low-lying spectrum of the ^{16}O nucleus using an α-cluster model which includes the important tetrahedral and square configurations. Our approach is motivated by the dynamics of α-particle scattering in the Skyrme model. We are able to replicate the large energy splitting that is observed between states of identical spin but opposite parities. We also provide a novel interpretation of the first excited state of ^{16}O and make predictions for the energies of 6^- states that have yet to be observed experimentally.

The energy spectrum of the Oxygen-16 nucleus has posed a challenge to nuclear physicists for decades. Wheeler suggested in the 1930s that one can model the nucleus as four α-particles with the ground state described as the particles in a tetrahedral arrangement [1]. This picture of the 0^+ ground state has been verified in many different models such as the shell [2, 3], lattice ab initio [4] and AMD [5] models, giving credence to the old cluster idea.

Despite the general agreement about the structure of the ground state, there is no consensus on the structure of the excited states of the nucleus. For example the first excited state, which has spin-parity 0^+, has been described as a four-particle-four-hole state [6], a breathing mode of the tetrahedron [7, 8], or correlated with a bent rhomb [9, 10] or square [4] arrangement of α-particles. The first suggestion has been put in doubt by more extensive studies [11], while the other three do not necessarily contradict each other − each model is simply too narrow in scope. The lattice spacing of the ab initio calculation [4] is too large to see the effect of the bent rhomb or breathing mode in detail. The algebraic model [8] only considers configurations near the tetrahedron and so does not include the square configuration. To resolve the disagreement about the 0^+ state one must study a model which includes large amplitude vibrations around the tetrahedron and allows for the rhomb-like and square configurations. In addition, this will remove a degeneracy of states seen in many models but not in the experimental spectrum.

The Skyrme model [12] is an effective field theory of hadrons arising as an approximate low-energy limit of QCD. It is a nonlinear theory of pions, whose small mass spontaneously breaks the chiral symmetry of the model. Nuclei are identified with solitons of the theory: the α-particle is described by a classical soliton with cubic symmetry. This allows for a spherically symmetric quantum ground state with spin-parity 0^+, matching conventional models [13]. It also reproduces α-clustering in larger nuclei [14, 15], such as ^{16}O. In particular it contains the tetrahedral and square configurations seen in conventional cluster models of ^{16}O.

The reason for using the Skyrme model is that it provides dynamics for the clusters. We can use this to construct a configuration space that we call the vibrational manifold. There is a dynamical mode, shown in Fig. 1, connecting the tetrahedral and square configurations, via bent rhomb configurations. Two pairs of α-particles approach each other and form a tetrahedron, which flattens out into a square, before reopening into the dual tetrahedron and then breaking into two pairs of α-particles again, having picked up a 90° twist. There are three of these modes passing through each tetrahedron, corresponding to the three pairs of opposing edges. If one starts at the tetrahedron and excites each of these modes equally then they will cancel out. Therefore there is degeneracy and these three modes only generate a two-dimensional space of configurations which forms our vibrational manifold.

This manifold is an extension of the linear E-vibrational space of the tetrahedron. It captures the low-energy path connecting the two tetrahedra via the

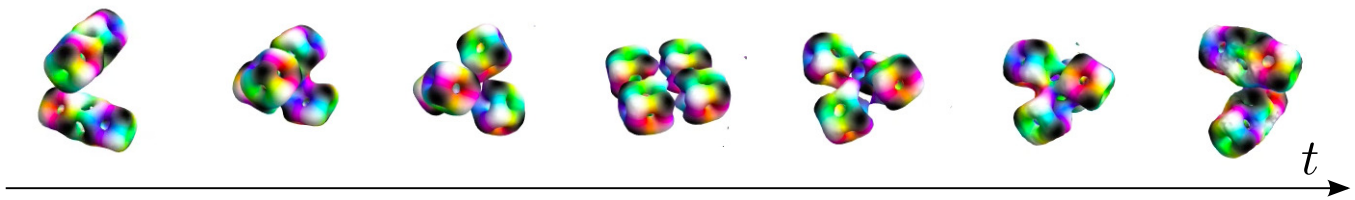

FIG. 1: A scattering mode of four α-particles in the Skyrme model. Each time step shows a surface of constant energy density which is coloured according to the field value as in [16].

square configuration as in Fig. 1. The presence of this path enables a significant energy difference to be created between quantum states with opposite parities, which would not be possible by only considering vibrations around the tetrahedron locally.

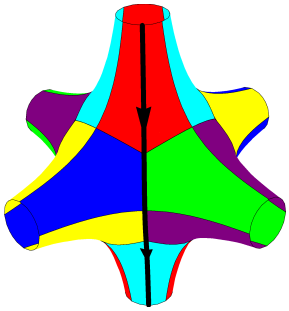

FIG. 2: The α-particles are restricted to lie on a surface with six punctures. Regions with the same colouring are related by D_2 symmetry. The scattering mode in Fig. 1 is represented by the thick black line.

The degrees of freedom in this vibrational manifold are the positions of the α-particles, which lie on a surface. To account for the asymptotics seen in Fig. 1, this surface must stretch out to infinity in six directions as in Fig. 2. Each configuration has D_2 symmetry and hence if one α-particle is at $\boldsymbol{x} = (x, y, z)$, the others are at $(x, -y, -z), (-x, y, -z)$ and $(-x, -y, z)$. This means we may focus on one quarter of the surface, which we denote by $\mathcal{M}$.

Having constructed the vibrational manifold we can now quantize the system using an extension of the scheme laid out in [17], but for the first time we include a two-dimensional manifold of configurations. The total configuration space is $\mathcal{M} \times SO(3)$, which allows for rotations of each configuration too. The quantum Hamiltonian is

$$\hat{H} = -\frac{\hbar^2}{2}\Delta + V(\boldsymbol{x}), \tag{1}$$

where $V(\boldsymbol{x})$ is the static energy of the configuration on $\mathcal{M}$ with an α-particle at $\boldsymbol{x}$, and the kinetic operator is proportional to the Laplace–Beltrami operator

$$\Delta = \det(g)^{-\frac{1}{2}}\partial_i\left(\det(g)^{\frac{1}{2}}g^{ij}\partial_j\right), \tag{2}$$

where g is the metric on $\mathcal{M} \times SO(3)$. The metric is block diagonal, because of the D_2 symmetry of the configurations, and hence the problem splits into vibrational and rotational parts. The total wavefunction is separable and can be written as

$$|\Psi\rangle = \sum_{L_3} \phi_{L_3}(\boldsymbol{x})\,|JL_3\rangle\,, \tag{3}$$

where ϕ is the vibrational wavefunction and $|JL_3\rangle$ are the rigid-body angular momentum states with spin J and body-fixed angular momentum projection L_3. In addition, the linear combination of states occurring in $|\Psi\rangle$ must be D_2 invariant.

The vibrational problem – The rescaled Schrödinger equation for the vibrational wavefunction is

$$-\Delta_{\text{vib}}\,\phi + V(\boldsymbol{x})\phi = (E - E_J)\phi\,, \tag{4}$$

where E is the total energy of $|\Psi\rangle$ and E_J is its rotational energy. E_J involves the moments of inertia of the configurations, which depend on the vibrational coordinates $\boldsymbol{x}$. However, for now, we consider them to be constant to simplify the calculation of the vibrational energy. We shall reinsert this dependence later in the paper.

To solve (4) we must first model the metric on our space $\mathcal{M}$. To do this we approximate $\mathcal{M}$ as one quarter of the 6-punctured sphere with constant negative curvature. This captures several important physical features of the system: that the particles can separate into pairs asymptotically and that the surface in Fig. 2 does indeed have negative curvature. The metric of this manifold is simple once we map $\mathcal{M}$ onto a sub-domain $\mathcal{F}$ of the complex upper half plane. For details, see [18]. The appropriate sub-domain for this problem is shown in Fig. 3. Defining $\zeta = \eta + i\epsilon$ as the complex coordinate on the upper half plane, the metric is then proportional to $\epsilon^{-2}\left(d\eta^2 + d\epsilon^2\right)$. This gives rise to the kinetic operator

$$-\Delta_{\text{vib}} = -\epsilon^2\left(\frac{\partial^2}{\partial\eta^2} + \frac{\partial^2}{\partial\epsilon^2}\right). \tag{5}$$

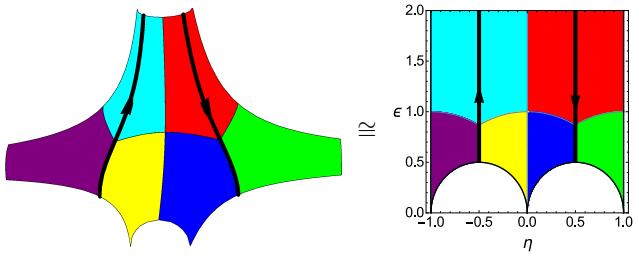

FIG. 3: The relation between $\mathcal{M}$ (left) and $\mathcal{F}$ (right). Tetrahedral configurations are at the points where three coloured regions meet while the square configurations are at points where four coloured regions meet. The scattering mode in Fig. 1 is represented by the thick black lines.

The 6-punctured sphere has cubic symmetry O and hence $\mathcal{M}$ has $O/D_2 \cong S_3$ symmetry, where S_3 is the permutation group of the x, y and z axes. S_3 can act on $\mathcal{M}$ or $\mathcal{F}$, permuting the coloured regions seen in Fig. 3. In addition, parity acts on $\mathcal{M}$ as

$$\boldsymbol{x} = (x, y, z) \to (-x, -y, -z) \equiv (x, -y, z) \tag{6}$$

where we have used the D_2 symmetry in the equivalence. This corresponds to $\eta \to -\eta$ on $\mathcal{F}$. Hence the vibrational wavefunctions fall into representations of S_3 and parity.

Our choice of potential V is motivated by cluster models which find that the tetrahedral configuration has the lowest energy [10]. Going towards the square or asymptotic configurations leads to a rise in potential energy.

In addition, we would like a potential for which (4) is soluble. A convenient candidate is

$$V(\eta,\epsilon) = \epsilon^2 \left(\omega^2 \left(\eta - \frac{1}{2} \right)^2 + \mu^2 \right) , \qquad (7)$$

where ω and μ are constant parameters and the ϵ^2 factor means that solutions of (4) are separable in η and ϵ.

This potential ansatz is a good approximation for the low-energy configurations but it diverges asymptotically for the separated pairs ($\epsilon \to \infty$). Bound states are concentrated around the tetrahedral and square configurations and so this divergence has a negligible effect on them. In order to study scattering states, a different potential that flattens out asymptotically would be required. The formula (7) only applies in the top right region of $\mathcal{F}$ and the potential elsewhere can be found by defining V to take the same value at points related by S_3.

Rovibrational states – The vibrational wavefunctions must be combined with spin states in order to form rovibrational states. The combinations that are permitted depend on the representation that the vibrational wavefunction falls into. There are two one-dimensional irreducible representations of S_3, known as the trivial and sign representations.

The two lowest-energy vibrational wavefunctions in the trivial representation are displayed in Fig. 4 (left and middle). When combined with the $|0,0\rangle$ spin state, we identify these solutions with the two lowest 0^+ states in the experimental spectrum of ^{16}O. The ground state is loosely concentrated around the two tetrahedral configurations in agreement with other models. The excited state has approximately equal concentration at the three square and the two tetrahedral configurations. Hence we deduce that a global analysis, including both tetrahedral and square configurations, is essential to explain the structure of the excited 0^+ state. These vibrational wavefunctions may also be combined with certain states of higher spin – those that have tetrahedral symmetry and positive parity. Overall, these wavefunctions give rise to a rotational band with spins $0^+, 4^+, 6^+, \ldots$.

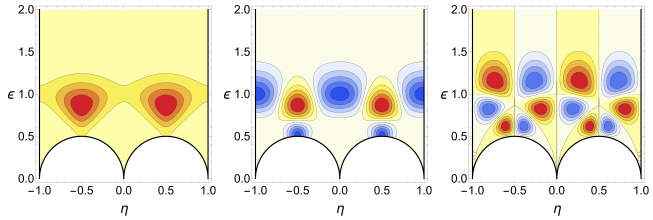

FIG. 4: Vibrational wavefunctions which lie in the trivial representation. From left to right: the ground state, the first excited state, and the lowest-lying state with negative parity.

If a configuration has a reflection symmetry and the wavefunction is non-zero there, one may calculate the intrinsic parity for a given spin state. For example, the tetrahedron has positive intrinsic parity for spins 0 and 4 but negative intrinsic parity for spin 3. This leads to constraints on the vibrational wavefunctions, one of which is that the spin 0 wavefunctions must take the same value at the tetrahedron and its dual. This is automatic for positive parity states as we can see in Fig. 4, noting that the parity operator for the vibrational wavefunctions corresponds to $\eta \to -\eta$. Negative parity wavefunctions are also permitted if they vanish at all configurations with a reflection symmetry. This is true of the rightmost wavefunction of Fig. 4 and hence one may combine it with a $|0,0\rangle$ spin state to give an overall 0^- state.

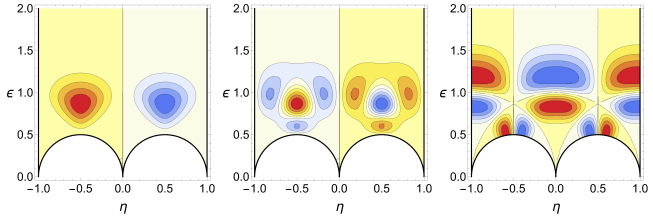

FIG. 5: Vibrational wavefunctions which lie in the sign representation. From left to right: the lowest-energy state, the first excited state, and the lowest-lying state with positive parity.

Vibrational wavefunctions in the sign representation of S_3 with negative (positive) parity are not too different from those in the trivial representation with positive (negative) parity. The sign representation wavefunctions are displayed in Fig. 5 and the similarities with those in Fig. 4 are manifest. The two wavefunctions on the left give rise to $3^-, 6^-, \ldots$ states while the right-most wavefunction gives rise to $3^+, 6^+, \ldots$ states of rather high energy.

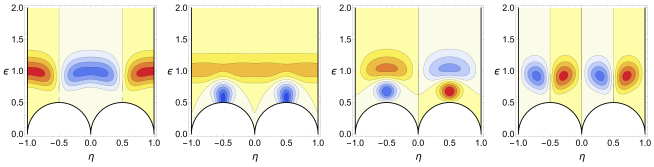

FIG. 6: The lowest-energy positive and negative parity vibrational wavefunctions which lie in the standard representation. From left to right: the functions ϕ_1 and ϕ_2 with positive parity, the functions ϕ_1 and ϕ_2 with negative parity.

The third and final irreducible representation of S_3 is the two-dimensional standard representation. Here the vibrational wavefunctions for a given eigenvalue have degeneracy two and we denote the orthogonal pair as ϕ_1 and ϕ_2. The lowest-energy positive and negative parity vibrational wavefunctions of this type are displayed in Fig. 6. The positive parity states are concentrated around the square configurations and hence give rise to approximate rotational bands of the square. The negative parity states have higher energy than the positive parity states since they are more constrained, having to

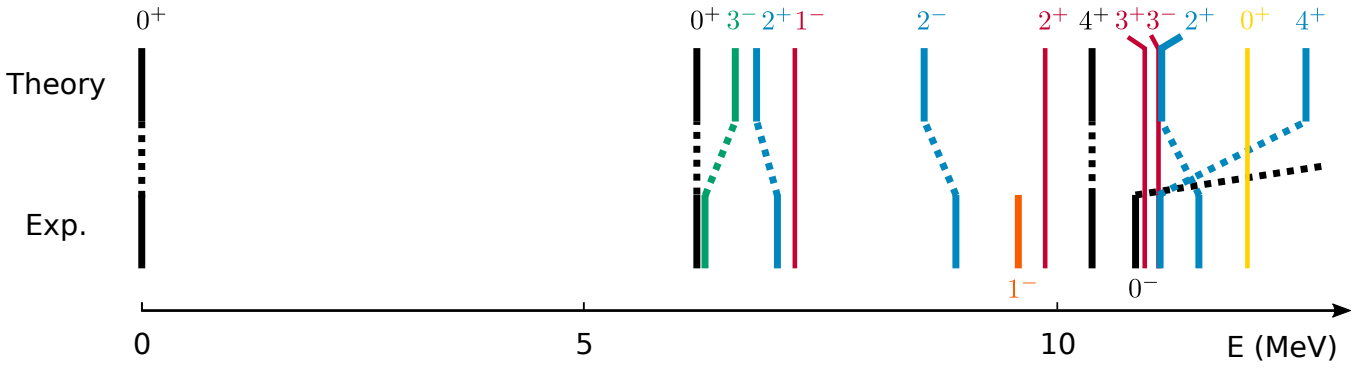

FIG. 7: The energy spectrum of our model up to 12.7 MeV compared with all the low-lying experimentally observed states [19]. States are coloured according to the type of vibrational wavefunction from which they arise. The partially dotted lines represent the trivial irrep (black), sign irrep (green) and standard irrep (blue) of S_3. Full vertical lines represent states identified with the F vibration (red) and A vibration (yellow). The 1^- state at 9.6 MeV is unexplained in our model.

vanish at the square configurations. As with the other representations, there are further vibrationally excited states which we have calculated though not displayed. These vibrational wavefunctions are then combined with a two-dimensional basis of spin states.

For spin 2 the total wavefunction is

$$|\Psi\rangle = \frac{\phi_1}{\sqrt{2}}\left(|2,2\rangle + |2,-2\rangle\right) + \phi_2\,|2,0\rangle\,. \qquad (8)$$

The vibrational wavefunctions ϕ_1 and ϕ_2 transform in the same way as the spin states they are paired with. Hence the total wavefunction is invariant under S_3 transformations and parity. We can construct similar states for spin-parity $J^P = 4^\pm, 5^\pm, 6^\pm, \ldots$.

The energy spectrum – In constructing the extended E-vibrational wavefunctions in (4) we neglected dependence of the moments of inertia on the vibrational coordinates. In order to calculate the rotational energy of our states we use an approximate inertia tensor that interpolates between the known values for the tetrahedral, square and asymptotic Skyrme model configurations shown in Fig. 1. This gives rise to a kinetic operator whose expectation value we then find. This is equivalent to using first order perturbation theory, which is justified as the energy gaps between vibrational states in the same representation are large.

While most of our analysis has focused on extending the E vibration of the tetrahedron, there are two other types of vibration that also need to be considered. The breathing, A vibration describes the four α-particles moving radially while preserving tetrahedral symmetry. It gives rise to excited $0^+, 3^-, 4^+, \ldots$ states. The F vibration contains the mode where one α-particle travels away from the other three, preserving C_3 symmetry. This allows for excited states of spin $1^-, 2^+, 3^\pm, 4^\pm, \ldots$.

The ^{16}O ground state is fixed at 0 MeV, with the excited 0^+ and lowest 4^+ state being used to scale the vibrational and rotational energy units respectively. The two remaining parameters (ω and μ) are chosen to give a good fit for the rest of the states. The first 15 states of the experimental spectrum are shown in Fig. 7 and after extracting those states coming from the A and F vibrations, we provide a good fit for most of the remaining states.

In particular, the lowest-lying 2^+ and 2^- states have the correct ordering, with a predicted energy gap of 1.8 MeV which is close to the experimentally observed gap of 1.96 MeV. This gap is caused by the vibrational wavefunctions having significantly different energies, due to their opposite parities. Our global analysis, including the tetrahedral and square configurations, is essential to describe this gap. The lowest 0^+, 3^- and 4^+ states still form a rotational band, despite the fact that the 3^- state has a different vibrational wavefunction (compare Fig. 5 with Fig. 4 (left)). For our choice of parameters in the potential, these vibrational wavefunctions have similar energies.

The calculated energy of the 0^- state in Fig. 4 is 16.35 MeV which is significantly larger than the lowest experimentally observed 0^- state which has energy 11.0 MeV. In our calculation we have used the potential (7) which diverges asymptotically; however, the configuration energy should flatten out as we approach the two separated pairs of α-particles ($\epsilon \to \infty$). Taking this into account would reduce the vibrational energy of all states but have a larger effect on highly excited states such as the 0^-.

We find a 6^+ state in the trivial S_3 representation at 21.7 MeV which agrees with an experimentally observed state at 21.6 MeV. In addition, we predict two 6^- states: one at 22.2 MeV from the sign representation and one at 27.1 MeV from the standard representation. Negative parity spin 6 states of ^{16}O have not yet been observed.

We do not provide an extended model of the F vibration as we have done with the E vibration, since previous studies have shown that a local, harmonic analysis describes the data well [7, 8]. Hence, we simply highlight the states arising from this vibration in Fig. 7 without calculating their energies. The A vibration splits the nucleus into four individual α-particles and hence its frequency must be large. We identify the state at 12.0 MeV as its first excitation.

Conclusion – We have considered an α-cluster model for ^{16}O with novel dynamics motivated by the Skyrme model. Our work allows for α-particle configurations with tetrahedral and square symmetry within a two-parameter family of configurations, going beyond the rigid body analysis considered previously [10], and also the harmonic analysis of the E vibration in [8]. The quantum Hamiltonian has a 0^+ ground state focused around the tetrahedral configuration in agreement with other models, but we provide a novel explanation for the excited 0^+ state as a superposition of the tetrahedral and square configurations. Our model allows a 0^- state which vanishes at the tetrahedral and square configurations, although these constraints give it a rather high energy. We also explain the energy gap between the low-lying 2^+ and 2^- states as being mainly due to their considerably different vibrational wavefunctions.

Acknowledgements – C. J. H. and C. K. are supported by STFC studentships.

*C.J.Halcrow@damtp.cam.ac.uk
†C.King@damtp.cam.ac.uk
‡N.S.Manton@damtp.cam.ac.uk

[1] J. A. Wheeler, Molecular viewpoints in nuclear structure. *Phys. Rev.* **52** (1937) 1083.
[2] J. K. Perring and T. H. R. Skyrme, The alpha-particle and shell models of the nucleus. *Proc. Phys. Soc. Lond.* **A69** (1956) 600.
[3] D. M. Brink and G. F. Nash, Excited states in Oxygen 16. *Nucl. Phys.* **40** (1963) 608.
[4] E. Epelbaum, H. Krebs, T. A. Lähde, D. Lee, U.-G. Meiβner and G. Rupak, Ab initio calculation of the spectrum and structure of ^{16}O. *Phys. Rev. Lett.* **112** (2014) 102501.
[5] Y. Kanada-En'yo and Y. Hidaka, Tetrahedral shape and surface density wave of ^{16}O caused by α-cluster correlations. *arXiv:1608.03642* (2016).
[6] W. H. Bassichis and G. Ripka, A Hartree-Fock calculation of excited states of O^{16}. *Phys. Lett.* **15** (1965) 320.
[7] D. M. Dennison, Energy levels of the O^{16} nucleus. *Phys. Rev.* **96** (1954) 378.
[8] R. Bijker and F. Iachello, Evidence for tetrahedral symmetry in ^{16}O. *Phys. Rev. Lett.* **112** (2014) 152501.
[9] D. M. Brink, H. Friedrich, A. Weiguny and C. W. Wong, Investigation of the alpha-particle model for light nuclei. *Phys. Lett.* **33B** (1970) 143.
[10] W. Bauhoff, H. Schultheis and R. Schultheis, Alpha cluster model and the spectrum of ^{16}O. *Phys. Rev.* **C29** (1984) 1046.
[11] J. M. Irvine, C. D. Latorre and V. F. E. Pucknell, The structure of ^{16}O; a review of the theory. *Adv. in Phys.* **20:88** (1971) 661.
[12] T. H. R. Skyrme, A non-linear field theory. *Proc. Roy. Soc. Lond.* **A260** (1961) 127.
[13] T. S. Walhout, Quantising the four baryon Skyrmion. *Nucl. Phys.* **A547** (1992) 423.
[14] R. Battye, N. S. Manton and P. Sutcliffe, Skyrmions and the α-particle model of nuclei. *Proc. Roy. Soc. Lond.* **A463** (2007) 261.
[15] P. H. C. Lau and N. S. Manton, States of Carbon-12 in the Skyrme model. *Phys. Rev. Lett.* **113** (2014) 232503.
[16] D. T. J. Feist, P. H. C. Lau and N. S. Manton, Skyrmions up to baryon number 108. *Phys. Rev.* **D87** (2013) 085034.
[17] C. J. Halcrow, Vibrational quantisation of the $B = 7$ Skyrmion. *Nucl. Phys.* **B904** (2016) 106.
[18] H. M. Farkas and I. Kra, Theta constants, Riemann surfaces and the modular group. (American Mathematical Society, Providence RI, 2001).
[19] J. H. Kelley, D. R. Tilley, H. R. Weller and C. M. Cheves, Energy levels of light nuclei $A = 16 - 17$. *Nucl. Phys.* **A564** (1993) 1.